PAPER • OPEN ACCESS

Collectively induced many-vortices topology via rotatory Dicke quantum phase transition

To cite this article: Priyam Das *et al* 2016 *New J. Phys.* **18** 093022

New Journal of Physics
The open access journal at the forefront of physics

Deutsche Physikalische Gesellschaft DPG
IOP Institute of Physics

Published in partnership with: Deutsche Physikalische Gesellschaft and the Institute of Physics

OPEN ACCESS

RECEIVED
28 April 2016

REVISED
3 August 2016

ACCEPTED FOR PUBLICATION
24 August 2016

PUBLISHED
9 September 2016

PAPER

Collectively induced many-vortices topology via rotatory Dicke quantum phase transition

Priyam Das[1], **Mehmet Emre Tasgin**[1] **and Özgür E Müstecaplıoğlu**[2]

[1] Institute of Nuclear Science, Hacettepe University, Ankara, 06800, Turkey
[2] Department of Physics, Koç University, Sarıyer, İstanbul, 34450, Turkey

E-mail: metasgin@hacettepe.edu.tr

Keywords: Bose–Einstein condensate, rotatory superradiance, Dicke quantum phase transition

Abstract

We examine the superradiance of a Bose–Einstein condensate pumped with a Laguerre–Gaussian laser of high winding number, e.g., $\ell = 7$. The laser beam transfers its orbital angular momentum (OAM) to the condensate at once due to the collectivity of the superradiance. An ℓ-fold rotational symmetric structure emerges with the rotatory superradiance. ℓ number of single-charge vortices appear at the arms of this structure. Even though the pump and the condensate profiles initially have cylindrical symmetry, we observe that it is broken to ℓ-fold rotational symmetry at the superradiance. Breaking of the cylindrical symmetry into the ℓ-fold symmetry and OAM transfer to the condensate become significant after the same critical pump strength. Reorganization of the condensate resembles the ordering in the experiment by Esslinger and colleagues (2010 *Nature* **264** 1301). We numerically verify that the critical point for the onset of the reorganization, as well as the properties of the emitted pulse, conform to the characteristics of superradiant quantum phase transition.

1. Introduction

Dicke superradiance (SR) is a fundamental effect that is the collective spontaneous emission of radiation by an ensemble of coherently excited atoms [1, 2]. The ensemble atoms are coupled together by a common electromagnetic field within the extent of the pump's coherence length, and are excited to phase synchronized multi-atom states. Cooperative rapid release of the stored energy leads to a so-called superradiant pulse with an intensity proportional to the square of the number of the atoms in the ensemble. The onset of SR is triggered by vacuum fluctuations in an empty photon mode, which stimulates strongly directional decay of atoms to this mode [3, 4] with a probability proportional to the exponential of the ensemble length along the emission direction [4].

In addition to dynamical SR, equilibrium SR can be studied as a first order quantum phase transition (PT) from a normal to cooperative radiation phase in finite systems [5]. Dicke SR quantum PT is proposed to occur in trapped, laser driven atomic Bose–Einstein condensates (BECs) in high finesse optical cavities [6]; and it is experimentally demonstrated [7]. Above a critical driving strength, SR PT happens simultaneously with the spatial fragmentation of the BEC into a periodical pattern. The collectivity in superradiant PT can be heralded by bi-partite quantum entanglement [8], single-mode non-classicality [9], and atomic (spin) squeezing [10] that can induce N-particle entanglement [11]. Collisions between atoms in BECs can also contribute to quantum entanglement and its interplay with the SR PT.

When an N atom BEC is stirred, it does not rotate until a total of $N\hbar$ orbital angular momentum (OAM) is transferred to it [12]. Instead of stirring, one can also control atomic center of motion to transfer OAM to a BEC using optical fields [13–16]. Such schemes operate at optical frequencies so that single atom recoil energy ($\hbar\omega_{\mathrm{R}}$) exceeds the mean atom–atom interaction energy (U_{int}/N). Though they cannot transfer the condensate to a rotatory state collectively, they can induce partial rotation on a BEC and yield vortex nucleation. In order to transfer sufficient OAM to generate vortices in a BEC, regular optical pumping schemes need two or more laser beams [13–18]. A BEC, which is pumped by a Laguerre–Gaussian (LG) beam with OAM, radiates by stimulated

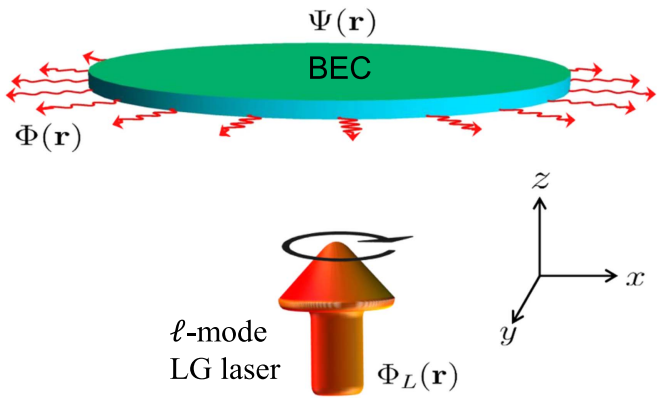

Figure 1. A pancake shaped BEC is illuminated with a strong LG laser of winding number ℓ with a profile $\Phi_{\rm L}(\mathbf{r})$ given in equation (1), carrying $\ell\hbar$ amount of OAM per photon. Above a critical pump strength $\eta > \eta_c$ BEC superradiates a field $\Phi(\mathbf{r})$ which is in the x–y plane due to thestrong confinementof BEC profile $\Psi(\mathbf{r})$ along the z-axis [33].

emission into a second laser in Gaussian (G) mode without any OAM [15]. Without using the G beam, high probability of emission into the pump beam relative to emission of zero OAM photons results in negligible OAM transfer into the BEC, which leads to weakly populated vortex side-mode.

In the present manuscript, we consider only a single LG pump beam, but with an intensity (or the BEC-field coupling) above a critical threshold at which SR with zero OAM occurs. Our idea is a generalization of the physical mechanisms behind Rayleigh [19] and Raman superradiance [20–22] from an off-resonant driven BEC in free space, which are the creation of density and spin polarization gratings, respectively [4, 23–25]. In our case recoiled condensate atoms form a ring grating, due to the conservation of linear momentum and interference of the recoiled matter waves. In addition, due to the OAM transfer, the grating is not frozen but rotating. The grating coherently overlaps with the condensate at rest. The contrast gets deeper with the more scattering, and in turn the scattered intensity is proportional to the square of the density contrast or to the square of the number of active atoms. Using large amount of OAM transfer at the threshold of 'rotatory' SR PT, weakly populated rotational symmetry broken field and vortex side modes can be coherently amplified which leads to significant nucleation of a 'vortex molecule' at the edge of the grating. The collective spontaneous emission character of the SR makes it fundamentally different than the known optical pumping schemes to transfer OAM to BEC, as the intensity of emission scales quadratically with the number of atoms inside the BEC, leading to larger amount of OAM transfer. From practical perspective SR scheme is also different, as it only uses a single pump laser beam. Besides, SR scheme can lead to complete transfer of BEC to rotational state by depleting the zero momentum condensate mode, in contrast to partial transfer achieved by regular two pump optical schemes.

Present contribution generalizes the case of superradiant generation of a single axial vortex along a cigar shaped BEC [26] to the superradiant generation of multiple vortices in a disk geometry and relaxes the condition of frozen spatial mode for the radiation field. Both the normal SR (without OAM transfer) and rotatory SR (with OAM transfer) can exhibit distinct behaviors in the small and large recoil regimes [26, 27]. When a cigar shaped BEC is pumped with an LG beam along its long axis, it is found that normal SR can either precede the rotatory SR in the small recoil regime or it can be completely suppressed by the rotatory SR in the large recoil regime when the LG pump width larger than the width of vortex side mode [26]. As the normal SR cannot lead to nucleation of vortices, we focus here only on rotatory SR. For brevity we use the term SR threshold for rotatory SR. Below the SR threshold, our scenario falls into the same case of single LG pump where emission of G-mode radiation, hence OAM transfer or vortex nucleation, is negligibly small; while above the SR threshold, cooperative emission of BEC atoms leads to enhancement of OAM transfer and vortex nucleation becomes significant. The rotatory SR threshold can be taken as an 'effective' vortex nucleation threshold in our scheme; though SR threshold and the critical threshold of vortex nucleation are different in principle and SR does not change the critical rotation threshold for vortex nucleation.

Our physical system is depicted in figure 1, where a pancake BEC is driven by an LG beam with winding number ℓ. Dynamical simulations of the model system show that single-charge vortices at the arms of the ℓ-fold symmetric structures becomes significant in the density profile of the BEC after SR threshold. We determine the intensity profile of the superradiant scattered pulse as well. Reorganization of the condensate into ℓ-fold rotational symmetric structures resembles SR induced spatial ordering of driven BEC in high finesse optical cavity [6, 7, 28–30], where the ordering arises due to the collective transfer of linear momentum via Dicke SR. Here, ℓ-fold rotational ordering and quantized vorticity emerge due to the OAM transfer to the BEC which is

enhanced via rotatory SR. Breaking of the cylindrical symmetry into the ℓ-fold symmetry and OAM transfer to the BEC become significant at the same critical pump strength. Quantized rotations (single-charge vortices) emerge at the edges of the ℓ-fold rotational ordered form. We tested the SR nature of the scattered radiation by verifying that the temporal width of the scattered pulse peak is inversely proportional to the number of atoms [31, 32]. In addition, peak intensity scales quadratically with the number of condensate atoms. Furthermore, we compared the dependence of the SR threshold on the radiation frequency and atom-field coupling to the case of SR of BEC in optical cavity [28] and find that they behave similarly.

This paper is organized as follows. In section 2 we present our model system, where we introduce and discuss the corresponding Hamiltonian and the equations of motion (EOM) in two subsections. Main results of the numerical simulations and their discussions are presented in section 3. Critical pump strength is discussed in more detail in section 4. We conclude in section 5.

2. Model system

We examine the dynamics of a pancake BEC of N atoms [33], as shown in figure 1, which is illuminated with a strong LG laser of optical frequency $\omega_{\rm L}$ along the symmetry axis z. The pump beam is well collimated with radial width $w_{\rm L}$ and propagates along the z-axis with a wave-vector $k_{\rm L}$. LG pumpmode is assumed to have a normalized spatial profile [34]

$$\Phi_{\rm L}(\mathbf{r}) = \frac{1}{\sqrt{\ell!\pi V_{\rm L}}}(r/w_{\rm L})^{\ell}\mathrm{e}^{-r^2/2w_{\rm L}^2}\mathrm{e}^{\mathrm{i}\ell\phi}\mathrm{e}^{\mathrm{i}k_{\rm L}z} \tag{1}$$

with zero azimuthal mode number and positive radial mode (winding) number $\ell > 0$. LG beam carries $\ell\hbar$ OAM per photon. Here, $V_{\rm L} = w_{\rm L}^2 z_{\rm L}$, with $z_{\rm L}$ being the mode quantization length. The electric field operator of the LG beam is given by

$$\hat{\mathbf{E}}_{\rm L}(\mathbf{r},\, t) = -\mathrm{i}\mathbf{e}_{\rm L}\mathcal{E}_{\rm L}\Phi_{\rm L}(r,\, \phi,\, z)\hat{a}_{\rm L}\mathrm{e}^{-\mathrm{i}\omega_{\rm L}t} + \mathrm{h.c.}, \tag{2}$$

where $\mathbf{e}_x$ is the unit polarization vector of the laser, $\mathcal{E}_{\rm L} = \sqrt{\hbar\omega_{\rm L}/2\epsilon_0}$, with ϵ_0 being the vacuum permittivity, and $\hat{a}_{\rm L}$ is the annihilation operator for the pump laser photons.

Similar to the end-fire modes emitted out of a pencil shaped condensate [4, 35], scattered radiation off a pancake BEC would consist of radial edge-fire modes, in the x–y plane shown in figure 1. End-fire modes are emitted along the radial directions since the BEC is tightly confined along the z-axis. When the x–y profile of the scattered radiation has a smaller winding number than the pump, OAM is transferred to the BEC.In the case of cooperative (SR) scattering, OAM is transferred to the BEC at once through an exponentially fast and collectively enhanced spontaneous emission [4]. We express the electric field operator of the scattered radiation as

$$\hat{\mathbf{E}}_{\rm s}(\mathbf{r},\, t) = -\mathrm{i}\mathbf{e}_{\rm s}\mathcal{E}_{\rm s}\hat{\Phi}(r,\, \phi,\, z;\, t)\mathrm{e}^{\mathrm{i}\mathbf{k}\cdot\mathbf{r}} + \mathrm{h.c.}, \tag{3}$$

where $\mathbf{e}_{\rm s}$ is the unit polarization vector of the scattered field; $\mathcal{E}_{\rm s} = \sqrt{\hbar\omega_{\rm e}/2\epsilon_0}$; $\omega_{\rm e}$ is the carrying end-fire mode frequency and $\hat{\Phi}(\mathbf{r})$ is the annihilation field operator for the scattered radiation. We include the factor $\exp(-\mathrm{i}\omega_{\rm e}t)$ into the field operator $\hat{\Phi}(\mathbf{r})$.

2.1. Hamiltonian

Assuming the LG beam is far off resonant from the atomic transition frequency, excited state can be adiabatically eliminated to describe the many body dynamics using an effective Hamiltonian [36, 37], $\hat{\mathcal{H}}$, which can be expressed as

$$\hat{\mathcal{H}} = \hat{\mathcal{H}}_0 + \hat{\mathcal{H}}_{\rm col} + \hat{\mathcal{H}}_f + \hat{\mathcal{H}}_{af} + \hat{\mathcal{H}}_{af}^{(2)}, \tag{4}$$

where

$$\hat{\mathcal{H}}_0 = \int \mathrm{d}^3\mathbf{r}\hat{\Psi}^{\dagger}(\mathbf{r})\hat{H}_g\hat{\Psi}(\mathbf{r}), \tag{5}$$

is the Hamiltonian of the external (motional) states of the BEC;

$$\hat{\mathcal{H}}_{\rm col} = g_{\rm s}\int \mathrm{d}^3\mathbf{r}\hat{\Psi}^{\dagger}(\mathbf{r})\hat{\Psi}^{\dagger}(\mathbf{r})\hat{\Psi}(\mathbf{r})\hat{\Psi}(\mathbf{r}), \tag{6}$$

is the interatomic collision Hamiltonian with $g_{\rm s}$ being the s-wave scattering strength;

$$\hat{\mathcal{H}}_f = \hbar\omega_{\rm e}\int \mathrm{d}^3\mathbf{r}\hat{\Phi}^{\dagger}(\mathbf{r})\hat{\Phi}(\mathbf{r}), \tag{7}$$

is the Hamiltonian of the scattered field;

$$\hat{\mathcal{H}}_{af} = \hbar g_a \int \mathrm{d}^3\mathbf{r}\hat{\Psi}^\dagger(\mathbf{r})\hat{\Phi}^\dagger(\mathbf{r})\alpha_{\mathrm{L}}\Phi_{\mathrm{L}}(\mathbf{r})\hat{\Psi}(\mathbf{r}) + \mathrm{h.c.}, \tag{8}$$

is the Hamiltonian of the scattering of the pump beam off the atoms with α_{L} being the c-number parametric approximation for the $\hat{a}_{\mathrm{L}}$; and

$$\hat{\mathcal{H}}^{(2)}_{af} = 2\hbar g_a \int \mathrm{d}^3\mathbf{r}\hat{\Psi}^\dagger(\mathbf{r})\hat{\Phi}^\dagger(\mathbf{r})\hat{\Phi}(\mathbf{r})\hat{\Psi}(\mathbf{r}), \tag{9}$$

is the Hamiltonian describing the interaction of the scattered field with the atoms. The first-quantized Hamiltonian of the BEC in a harmonic potential $V(r)$, with radial and axial trapping frequencies ω_r and ω_z, respectively, is given by $\hat{H}_g = -\hbar^2\nabla^2/2m + V(r)$. The effective strength of the atom-field interaction is denoted by g_a.

In general, the interaction strengths in equations (8) and (9) are different. Instead of g_a, we could write g_b in equation (9). They are given by $g_a = g_{\mathrm{L}}g_{\mathrm{e}}/\Delta_a$, and $g_b = g_{\mathrm{e}}^2/\Delta_a$ [7, 28, 36, 37], where $\Delta_a = \omega_a - \omega_{\mathrm{L}}$ is the detuning of the pump frequency from the atomic transition frequency ω_a; $g_{\mathrm{L}} = d_{\mathrm{L}}\mathcal{E}_{\mathrm{L}}/\hbar$ and $g_{\mathrm{e}} = d_{\mathrm{e}}\mathcal{E}_{\mathrm{s}}/\hbar$ are the single photon Rabi frequencies for the laser and scattered field, respectively. For simplicity we take $\mathbf{e}_{\mathrm{L}} = \mathbf{e}_{\mathrm{s}}$. Different polarizations, including the radial one, can be synthesized using linearly polarized LG beams [38]. Accordingly, we can take $d_{\mathrm{L}} = d_{\mathrm{e}}$, where d_{L} and d_{e} are the matrix elements of the atomic dipole moment operator components along $\mathbf{e}_{\mathrm{L}}$ and $\mathbf{e}_{\mathrm{s}}$, respectively. Due to the energy conservation in Rayleigh scattering, and small atomic side mode energies relative to the pump laser energy, pump and scattered field are in quasi-resonance, $\omega_{\mathrm{L}} \approx \omega_{\mathrm{e}}$. In fact, frequency dependence of the coupling constants is neglected over wider range of field detuning $\Delta = \omega_{\mathrm{e}} - \omega_{\mathrm{L}}$, which is the case in SR of BEC in optical cavity [7, 28, 36, 37]. Under these conditions describing our physical system, we find that $g_a = g_b$. We scale the BEC wave-function $\Psi(\mathbf{r})$ and the scattered field $\Phi(\mathbf{r})$ with $\sqrt{N}$ [28]. Parameters $\eta = g_a\sqrt{N}|\alpha_{\mathrm{L}}|$ and $U_0 = g_a N$ reflect the strength of the $\hat{\mathcal{H}}_{af}$ and $\hat{\mathcal{H}}^{(2)}_{af}$ atom-field couplings, respectively on the dynamics of scaled BEC and scattered field profiles. The physical condition of $g_a = g_b$ hence has no restrictive effect on the control of the dynamics in terms of independent parameters η and U_0.

The dynamics of the field operator for the scattered pulse $\hat{\Phi}(\mathbf{r})$ and the field operator of the BEC $\hat{\Psi}(\mathbf{r})$ will be determined by the EOM.

2.2. Equations of motion

Due to the symmetry of the system and the form of the pump (1), we make separation of variables in the BEC and the field operators, $\hat{\Psi}(r) = \hat{\psi}(x, y)\hat{Z}(z)$ and $\hat{\Phi}(r) = \hat{F}(x, y)Z_f(z)$. This reduces the computational efforts significantly. We obtain the time evolution for each operator using the Heisenberg EOM, which is given in the appendix, and solve the coupled equations numerically in the mean field limit for the field amplitudes where we replace the operators by c-numbers.

Scattering of the pump beam off the BEC, described by $\hat{\mathcal{H}}_{af}$, favors the macroscopic occupation of the scattered field [5], while energy of the $\hat{\mathcal{H}}^{(2)}_{af}$ is minimized with a minimum scattered field. Hence, $\hat{\mathcal{H}}_{af}$ and $\hat{\mathcal{H}}^{(2)}_{af}$ work against each other. If g_s is negative (positive), collision term supports (works against) the SR transition [6, 28]. In [28] the form of the scattered pulse becomes a simple function, i.e. cos(kx). In our case, it is not trivial to predict a frozen spatial mode approximation which can maximize or minimize the interactions properly or to use a few terms in the mode expansions of BEC and scattered field profiles. Hence, we do not make any mode expansion in the BEC, $\Psi(\mathbf{r})$, or in the scattered SR field, $\hat{F}(x, y)$, profiles.This allows us to numerically develop their mutually consistent evolution through the EOM.

Tightly confined pancake BEC does not superradiate along the z-direction. The scattered light mainly consists of the end-fire modes propagating in the x–y plane, due to the strong directionality of the SR [4, 39], thus it has no component along the z-direction. Therefore, we drop z dependence, $Z_f(z)$, of field profile $\Phi(\mathbf{r})$. Additionally, again due to the tight confinement of the BEC along the z-direction, vortices pointing along the x–y directions are energetically unfavorable.

We examine the behavior of the system both in the presence and the absence of damping. Following the mean field theory of free space SR from an ensemble of atoms, we introduce a phenomenological linear loss term into the field dynamical equation in our Maxwell–Bloch typemean field equations [29, 40, 41], in equation (A1). Presence of dampingincreases the critical threshold of SR at which significant OAM transfer and ℓ-fold ordering emerge. In semiclassical Maxwell–Bloch treatment of SR dynamics of low dimensional finite systems, phenomenological damping parameter to the radiation field is always introduced [40] to represent linear or diffraction losses [42] or to model escape of photons from an active cavity region [43]. In more recent mean field treatments of SR from trapped BECs [20, 35], a similar linear loss parameter as effective decay rate of the field is also used to compensate the neglect of propagation of the radiation field in the mean field description. Following

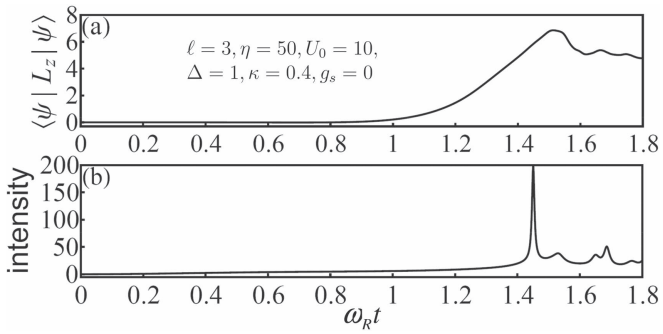

Figure 2. (a) OAM transfer to the BEC pumped continuously by an LG beam follows the (b) scattering peak (rotatory SR) at $t \simeq 1.45/\omega_R$. Reorganization of the BEC profile, from azimuthal symmetry to ℓ-fold rotational symmetry, with ℓ quantized vortices, emerges close before the intensity peak.

these standard treatments, we introduce a phenomenological linear loss parameter as well. The range of values we systematically used for κ to test robustness of our results are in the same range with the linear loss parameter used in the theoretical descriptions [23, 35] of the free space SR of BEC experiment [19]. Even though it is not a fundamental ingredient of the physics of superradiant OAM transfer to BEC or symmetry breaking, it can represent various experimental scenarios and allows us to analyze the robustness of our results and to make a more complete comparison with the behavior in the analytical formula of the critical coupling strength given in [6, 28]. More specifically, it is analytically found that effective field decay rate parameter for the free space SR experiment [19] is in the order of $\kappa \sim 10^4$ Hz [23]. We use time and frequency scaling in our EOM in terms of the recoil frequency $\omega_R \sim 10^5$ Hz [19], which gives a dimensionless $\kappa \sim 0.1$. We tested robustness of our results using values up to $\kappa \sim 3$ in our simulations.

3. Vortices with ℓ-fold rotational symmetry

We evolve $F(x, y)$ and $\Psi(\mathbf{r}) = \psi(x, y)Z(z)$ using the EOM given in the appendix in dimensionless time scaled by ω_R. In figure 2, macroscopic OAM transfer to the BEC follows the emission peak (at $t \simeq 1.45/\omega_R$). In figure 2(a), the $\langle\hat{L}_z\rangle$ can have values different than pump LG photon's OAM due to collective nature of the superradiant scattering. We calculated the OAM of the scattered field $F(x, y)$. We find that it always remains close to zero ($\sim 10^{-5}$). The difference between the BEC sample OAM and the pump LG photon OAM is not due to the scattered field OAM. BEC atoms act as a single object and scatter pump photons collectively. Each absorbed pump photon transfers $\ell\hbar$ amount of OAM to the BEC. BEC OAM is determined by the total contribution of a fraction of pump photons. The OAM that can be received collectively by the N-atom BEC must be an integer multiple of $\hbar$ per atom so that we can express it as $nN\hbar$, where n is an integer. The fraction of absorbed pump photons is then given by nN/ℓ. Accordingly the number of scattered photons per atom, n/ℓ, can be different than one in the collective scattering.

The temporal width $\Delta\tau$ of the peak in figure 2(b) exhibits the characteristic superradiant behavior [31, 32]. When we increase the number of atoms by n times, temporal width of the peak shrinks to $\Delta\tau/n$, as can be seen in figure 3. In addition, the peak intensitygrows quadratically with the number of BEC atoms, $\propto N^2$, which is another signature of SR [31, 32]. Hence, we conclude that the scattering displays the superradiant character.

In figure 4, we depict the time evolution of the spatial profile for both the BEC and the scattered field. In the close proximity of the scattering peak, figure 2(b), azimuthal symmetric BEC profile reorganizes to 3-fold rotational symmetry, figure 4(b). This happens even though both BEC and LG pump intensity have cylindrical symmetry initially. The winding number of the laser is transformed to the 3-fold rotational symmetry. Three single-charge vortices appear at the arms of the 3-fold rotational symmetric density profile. By enclosing small spatial regions around the three vortex positions, we calculate the expectation value of the $\hat{L}_z$ operator and find that they carry a single charge. In figure 4(d), we observe the expansion of the three vortices when the laser field isturned off. Remaining OAM $(m_{\text{tot}} - \ell)\hbar$, per atom, is distributed to the body of the BEC, where $m_{\text{tot}} = \langle\Psi(\mathbf{r})|\hat{L}_z|\Psi(\mathbf{r})\rangle$ is the total OAM of the BEC (per atom, due to the scaling of the $\Psi(\mathbf{r})$.

In our simulations, ℓ-fold rotational symmetric structures are significantin a BEC which is pumped with an LG laser of winding number ℓ only when $\eta > \eta_c$, as exemplified in figure 5. Single-charge vortices emerge at the ends of ℓ-fold rotational symmetric structures,and shown in figure 5 when the pump is switched off. When the OAM transferred to BEC is smaller than the ℓ-fold symmetry, $m_{\text{tot}} < \ell$, ℓ-fold symmetric structures emerge again. However, in this case no single-charge vortex appear at the arms The whole OAM is distributed to the

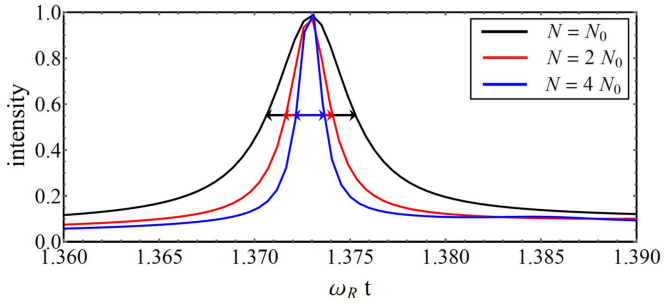

Figure 3. The temporal widths of the pulse peaks are proportional to $1/N$,which is a characteristic of a SR pulse [31]. We observe that FWHM is $\Delta\tau = 0.0048$ for $N = N_0 = 10^6$; $\Delta\tau = 0.0023$ for $N = 2N_0$ and $\Delta\tau = 0.0012$ for $N = 4N_0$. We remind that N appears in the parameters as $\eta = g_a\sqrt{N}|\alpha_L|$ and $U_0 = g_a N$. (We shifted the three curves to the same peak position and normalized the max intensity to 1 and no damping is assumed.)

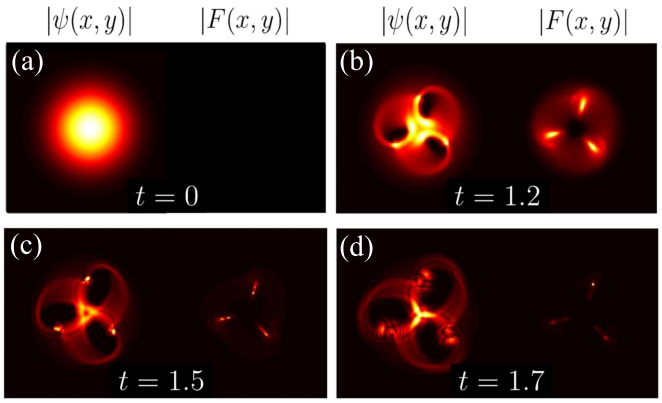

Figure 4. Time evolution of the profiles (corresponding to figure 2) of the BEC $|\psi(x, y)|$ and the scattered field $|F(x, y)|$ for pumping with an $\ell = 3$ mode LG laser above the critical pump strength $\eta > \eta_c$. To increase visibility of sharp peaks, we choose to plot absolute values of the profile functions instead of their absolute squares. 3-fold rotational symmetric structures appear (b) both in the BEC and scattered field, even though both have cylindrical symmetry initially. (c) Single-charge vortices appear at the ends of the structure such that (d) expansion of the vortices can be observed when the laser is turned off at $t \simeq 1.51/\omega_R$. Quantized vortices appear suddenly when $m_{tot} > 3$. In (c) and (d), scattered field are very sharp, so that graphs look as if they are faded due to the scaling of the colormap.

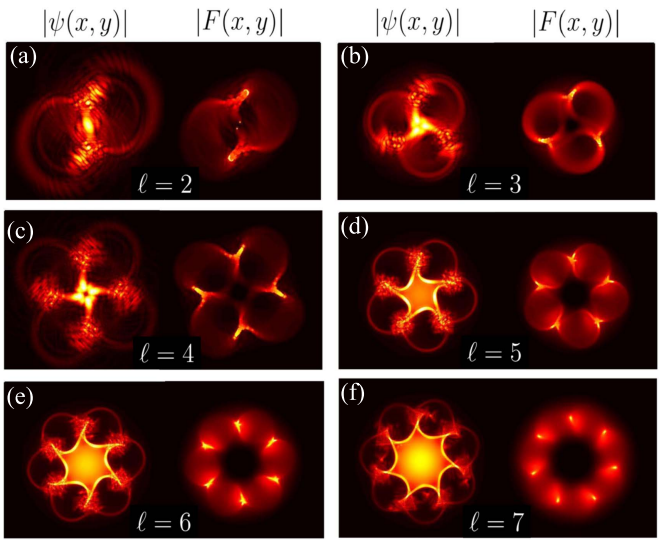

Figure 5. ℓ-fold rotational symmetric structures emerge for pumping with LG laser, profile (1), of winding number ℓ. ℓ number of single-charge vortices appear at the ends of ℓ-fold structures above a critical pump strength of the ℓ-mode LG laser. η values are 50, 60, 70, 120, 120, 150 and the times profiles belong to are $t = 2.2,\ 1.4,\ 1.56,\ 0.39,\ 0.23,\ 0.15$, respectively, and even a higher value of damping is chosen, $\kappa = 3$.To increase visibility of sharp peaks, we choose to plot absolute values of the profile functions instead of their absolute squares.

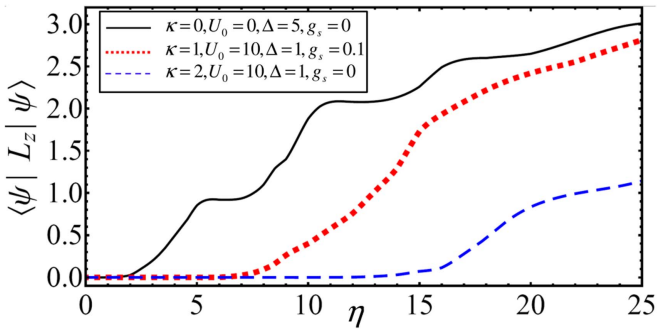

Figure 6. OAM transfer to the BEC, pumped by an LG beam with $\ell = 3$, can be achieved only after a critical pump strength $\eta > \eta_c$, which depends on the actual values of end-fire mode frequency (Δ), diagonal atom-field coupling (U_0), damping (κ) and atom–atom collisions (g_s). The solid line remains zero up to the critical value of $\eta_c = 2.25$.

body of the BEC. No quantized vorticity can be identified in the body of the BEC. In our case of pure rotatory SR scattered field OAM cannot be used to probe BEC OAM, as it has no OAM. On the other hand, it could be used to probe cylindrical symmetry breaking. Scattered field intensity profile carries information on the cylindrical symmetry breaking of BEC as figures 4 and 5 demonstrate. In our treatment there is no stimulating secondary Gaussian beam that would impose a specific profile on the scattered field. Accordingly, we do not make frozen spatial profile or few mode expansion approximations but we let the spatial profiles of the scattered field and the BEC evolve consistently by the coupled EOM. The interplay in their mutual evolution allows us to use scattered field profile as a probe for BEC profile. The intensity profile of the scattered field exhibits the similar dynamical development as symmetry breaking in BEC. The scattered field does not show ℓ-fold ordering patterns if $\eta < \eta_c$. Hence it can be used as an alternative probe for the dynamics of rotational self-organization and symmetry breaking in BEC.

4. Critical pump strength

In figure 6, we observe that OAM transfer to the BEC can be achievedby using a single LG pump only above a critical pump strength η_c depending on the values of the parameters U_0, g_s and κ, similar to the Dicke SR of BEC in optical cavity [28]. This behavior can be compared with figure 7. The 3-fold ordering in the BEC profile start to grow with η visibly after η_c as can be seen in figure 7, in parallel with the figure 6, showing increasing OAM transfer to the BEC above the threshold η_c to macroscopically large values[3].

In the absence of damping, $\kappa = 0$, we clearly observe the staircase of plateaus at $\langle \hat{L}_z \rangle = 1$ and $\langle \hat{L}_z \rangle = 2$ horizontal lines. This resistance against the OAM transfer is due to the irrotational nature—unless integer multiplies of $N\hbar$ OAM is gained [12]—of the BEC. When we introduce damping, these plateaus tend to disappear.

In figure 6, we observe a smooth increase in the OAM transferred to the BEC.Let us note that when we say OAM transfer to the BEC with non-integer $\langle \hat{L}_z \rangle$ values, we mean that BEC can have transient OAM values in real time dynamics only for a short time unlike quantized vorticity. We emphasize that, for $\eta < \eta_c$, BEC does not have OAM even for a short time. Despite the smooth increase in $\langle \hat{L}_z \rangle$, the visibility of the ℓ-fold rotational ordering appears quite sharply just after $\eta > \eta_c \simeq 2.25$. In figure 7, we observe that between $\eta = 1.50$–2.25, visibility of the 3-fold ordering remains almost constant and low, while for $\eta > \eta_c \simeq 2.25$, visibility of 3-fold ordering grows towards $\eta \sim 5$, in parallel with the behavior in figure 6. Therefore, onset of the OAM transfer to the BECdetermines when 3-fold rotational symmetric ordering becomes significant (see footnote 3).

Even though the complexity of the functions determining the superradiant emission and the recoiled BEC prevents us from establishing a simple analytical expression for the threshold η_c, we can make numerical comparison with the known behavior of the SR threshold with system parameters [6, 7, 28]. In figure 8, we present logarithmic plots showing behaviors of η_c with U_0 and Δ. We observe that $\eta_c \sim \Delta^{1/2}$ and $\eta_c \sim U_0^{1/2}$, for non-interacting BEC, as expected behaviors by the analytical predictions of SR threshold [28]. According to [28], $\eta_c \sim U_0^{1/2}$ behavior should be observed for the large values of U_0 and hence we consider a domain of U_0 in figure 8 so that $\Delta = 1$ can be neglected in this regime.

[3] It is worth noting that sudden jumps in order parameters appear when the order parameter is plotted with respect to the as in figure 1 of [28]. When we plot the time evolution of the order parameter for $\eta > \eta_c$, in [28],we do not observe such sudden jumps in the order parameter. Similarly, quantized vorticity appears smoothly in the time evolution [46, 47].

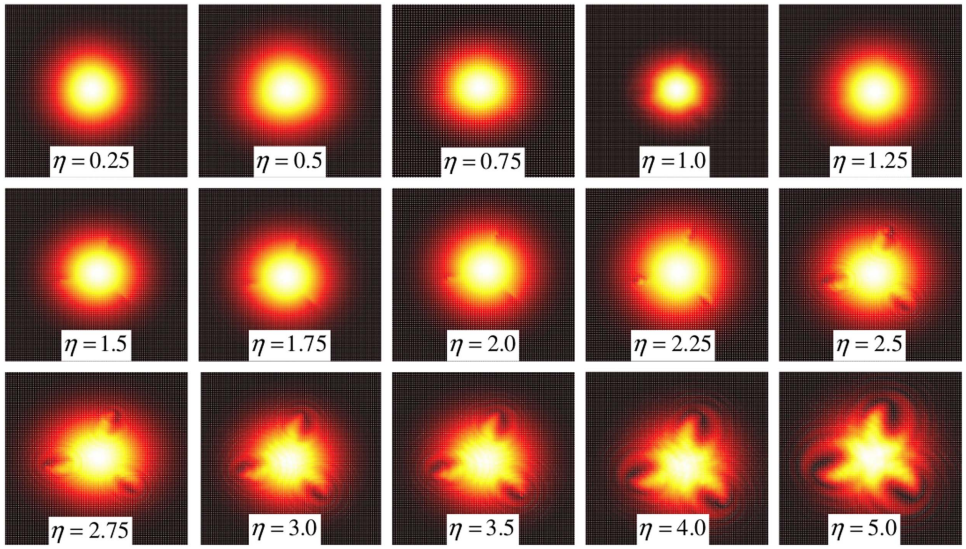

Figure 7. Visibility of the 3-fold rotational ordering in the BEC profile ($|\psi(x, y)|$) for different η values. To increase visibility of sharp peaks, we choose to plot absolute values of the profile functions instead of their absolute squares. Profiles correspond to solid line in figure 6. For each η value, we perform the time evolution and capture the BEC profile where 3-fold ordering is most visible. Above $\eta = \eta_c \simeq 2.25$ the visibility of the 3-fold symmetry jumps. Only after $\eta > \eta_c = 2.25$, OAM transfer to BEC can be achieved as shown in figure 6. For $\eta < \eta_c$, BEC cannot have OAM even for a short time.

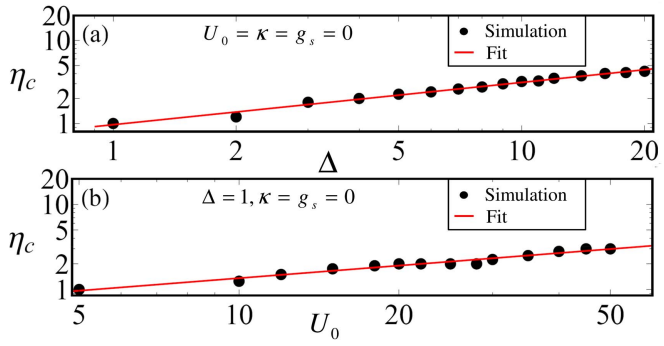

Figure 8. Dependence of the critical pump strength η_c on the (a) end-fire mode frequency Δ and (b) on the atom-field coupling U_0. The slopes of the log–log plots are 0.509 and 0.489, respectively, which indicates the behavior $\eta_c \sim \Delta^{1/2}$ and $\eta_c \sim U_0^{1/2}$ as predicted by the model of Nagy *et al* [6, 28].

5. Conclusion

In summary, we numerically observe that when a pancake shaped BEC is pumped with a single LG beam of winding number ℓ, it significantly reorganizes to ℓ-fold rotational symmetry above the critical pump strength for rotatory SR, η_c. For $\eta < \eta_c$, OAM transfer to the BEC is negligible. When $\eta > \eta_c$, both OAM transfer (see footnote 3) and ℓ-fold rotational symmetry become significant simultaneously. For excess OAM transfer, ℓ number of single-charge vortices appear at the arms of the ℓ-fold symmetric structures. In the time evolution, these structures develop visibly after a sharp SR scattering peak. The temporal width and the maximum of the peak conform to the SR characteristics [31, 32].

In this contribution, we limit our discussion to free space SR and do not consider the case of trapping the SR scattered pulse in a cavity in the x–y directions. In order to consider confined fields configuration, one can envision a system where a high finesse optical cavity is placed around the BEC [7]. In such a case one can imagine that the onset of the SR phase could also induce structural PT in translational degrees of freedom leading to a crystalline structure in the BEC, or a 'supersolid'. In other words, before SR induced rotational PT, there could be a supersolid phase. On the other hand, one can also imagine that, due to different thresholds for rotational and translational symmetry breaking, depending on system parameters a rotational transition can happen first. In addition, translational symmetry breaking could accompany the rotational ordering, too. In our opinion such a rich optical and structural phase diagram requires a separate study, including detailed examination of the phase

boundaries and the onset of normal and rotatory SR regimes with second quantized approaches. Different mechanisms to generate supersolid vortex crystals are proposed in literature such as in Rydberg-Dressed BECs where supersolid and vortex lattice phases are found [44]. Our choice of free space SR case is only for clarity and simplicity to eliminate translational symmetry breaking to focus on generation of multiple vortices topologies.

Our results can be significant to probe vortex nucleation and rotational symmetry breaking dynamics using the scattered radiation, and as an alternative single optical pumping scheme for rapid and large OAM transfer to BEC. We hope our scheme can inspire further investigation directions such as cavity confinement effects [7], supersolidity and bosonic vortex molecules and crystals [44], and collective excitations [45].

Acknowledgments

The authors thank L You and L Deng for illuminating discussions and acknowledge the financial support from TUBITAK Projects Grant No. 112T927 and 114F170. ÖEM acknowledge support from TUBITAK Project Grant No. 112T974.

Appendix A. Equations of motion

EOMs transforms to the following in the scaled form, where time and energy (frequency) scale is the recoil frequency, which is taken to be the same with the radial trapping frequency ω_r, determining the spatial scaling

$$\mathrm{i}\frac{\mathrm{d}F(x,y)}{\mathrm{d}t} = (-\mathrm{i}\kappa + \Delta)F(x,y) + \eta|\psi(x,y)|^2 F_{\mathrm{L}}(x,y)\int|Z(z)|^2\mathrm{d}z + 2U_0F(x,y)|\psi(x,y)|^2\int|Z(z)|^2\mathrm{d}z \tag{A1}$$

$$\begin{aligned}\mathrm{i}\frac{\mathrm{d}\psi(x,y)}{\mathrm{d}t} &= \eta(F_{\mathrm{L}}(x,y)F^*(x,y) + F_{\mathrm{L}}^*(x,y)F(x,y))\psi(x,y)\int|Z(z)|^2\mathrm{d}z \\ &+ 2U_0\psi(x,y)|F(x,y)|^2\int|Z(z)|^2\mathrm{d}z + \bar{g}_{\mathrm{s}}|\psi(x,y)|^2\psi(x,y)\int|Z(z)|^4\mathrm{d}z \\ &- \frac{1}{2}[(\partial_x^2+\partial_y^2)\psi(x,y)]\int|Z(z)|^2\mathrm{d}z - \frac{1}{2}\psi(x,y)\int Z^*(z)\partial_z^2Z(z)\mathrm{d}z \\ &+ \frac{1}{2}(x^2+y^2)\psi(x,y)\int|Z(z)|^2\mathrm{d}z + \frac{1}{2}\left(\frac{\omega_z}{\omega_r}\right)^2\psi(x,y)\int z^2|Z(z)|^2\mathrm{d}z,\end{aligned} \tag{A2}$$

$$\begin{aligned}\mathrm{i}\frac{\mathrm{d}Z(z)}{\mathrm{d}t} &= \eta Z(z)\int(|\psi(x,y)|^2F_{\mathrm{L}}(x,y)F^*(x,y) + |\psi(x,y)|^2F_{\mathrm{L}}^*(x,y)F(x,y))\mathrm{d}^2r \\ &+ 2U_0Z(z)\int|\psi(x,y)|^2|F(x,y)|^2\mathrm{d}^2r + \bar{g}_{\mathrm{s}}|Z(z)|^2Z(z)\int|\psi(x,y)|^4\mathrm{d}^2r \\ &- \frac{1}{2}Z(z)\int\psi^*(x,y)(\partial_x^2+\partial_y^2)\psi(x,y)\mathrm{d}^2r - \frac{1}{2}\partial_z^2Z(z)\int|\psi(x,y)|^2\mathrm{d}^2r \\ &+ \frac{1}{2}Z(z)\int(x^2+y^2)|\psi(x,y)|^2\mathrm{d}^2r \\ &+ \frac{1}{2}\left(\frac{\omega_z}{\omega_r}\right)^2z^2Z(z)\int|\psi(x,y)|^2\mathrm{d}^2r.\end{aligned} \tag{A3}$$

References

[1] Dicke R H 1954 *Phys. Rev.* **93** 99
[2] Skribanowitz N, Herman I, MacGillivray J and Feld M 1973 *Phys. Rev. Lett.* **30** 309
[3] Andreev A V, Emel'yanov V I and Il'inskii Y A 1993 *Cooperative Effects in Optics: Superradiance and Phase Transitions* (Bristol: IOP)
[4] Moore M G and Meystre P 1999 *Phys. Rev. Lett.* **83** 5202
[5] Emary C and Brandes T 2003 *Phys. Rev. Lett.* **90** 044101
[6] Nagy D, Kónya G, Szirmai G and Domokos P 2010 *Phys. Rev. Lett.* **104** 130401
[7] Baumann K, Guerlin C, Brennecke F and Esslinger T 2010 *Nature* **464** 1301
[8] Lambert N, Emary C and Brandes T 2004 *Phys. Rev. Lett.* **92** 073602
[9] Tasgin M E 2015 arXiv:1502.00992
[10] Yukalov V I and Yukalova E P 2004 *Phys. Rev.* A **70** 053828
[11] Sørensen A, Duan L-M, Cirac J and Zoller P 2001 *Nature* **409** 63
[12] Pethick C J and Smith H 2002 *Bose–Einstein Condensation in Dilute Gases* (Cambridge: Cambridge University Press)
[13] Tabosa J W R and Petrov D V 1999 *Phys. Rev. Lett.* **83** 4967
[14] Andersen M F, Ryu C, Cladé P, Natarajan V, Vaziri A, Helmerson K and Phillips W D 2006 *Phys. Rev. Lett.* **97** 170406
[15] Wright K C, Leslie L S and Bigelow N P 2008 *Phys. Rev.* A **77** 041601
[16] Moretti D, Felinto D and Tabosa J W R 2009 *Phys. Rev.* A **79** 023825

[17] Mondal P K, Deb B and Majumder S 2015 *Phys. Rev.* A **92** 043603
[18] Bhowmik A, Mondal P K, Majumder S and Deb B 2016 *Phys. Rev.* A **93** 063852
[19] Inouye S, Chikkatur A, Stamper-Kurn D, Stenger J, Pritchard D and Ketterle W 1999 *Science* **285** 571
[20] Wang T and Yelin S F 2005 *Phys. Rev.* A **72** 043804
[21] Schneble D, Campbell G K, Streed E W, Boyd M, Pritchard D E and Ketterle W 2004 *Phys. Rev.* A **69** 041601
[22] Yoshikawa Y, Sugiura T, Torii Y and Kuga T 2004 *Phys. Rev.* A **69** 041603
[23] Piovella N, Bonifacio R, McNeil B W J and Robb G R M 2001 *Opt. Commun.* **187** 165
[24] Bonifacio R, Cataliotti F S, Cola M, Fallani L, Fort C, Piovella N and Inguscio M 2004 *Opt. Commun.* **233** 155
[25] Uys H and Meystre P 2007 *Phys. Rev.* A **75** 033805
[26] Tasgin M E, Mustecaplioglu O E and You L 2011 *Phys. Rev.* A **84** 063628
[27] Hang C, Gabadadze G and Huang G 2015 *Phys. Rev.* A **92** 033805
[28] Nagy D, Szirmai G and Domokos P 2008 *Euro. Phys. J.* D **48** 127
[29] Öztop B, Bordyuh M, Müstecaplıoğlu Ö E and Türeci H E 2012 *New J. Phys.* **14** 085011
[30] Safaei S, Müstecaplıoğlu Ö E and Tanatar B 2013 *New J. Phys.* **15** 083037
[31] Mandel L and Wolf E 1995 *Optical Coherence and Quantum Optics* (Cambridge: Cambridge University Press)
[32] Bonifacio R and Lugiato L 1975 *Phys. Rev.* A **11** 1507
[33] Gopalakrishnan S, Lev B L and Goldbart P M 2009 *Nat. Phys.* **5** 845
[34] Kanamoto R, Wright E M and Meystre P 2007 *Phys. Rev.* A **75** 063623
[35] Müstecaplioğlu O E and You L 2000 *Phys. Rev.* A **62** 063615
[36] Moore M, Zobay O and Meystre P 1999 *Phys. Rev.* A **60** 1491
[37] Tasgin M E 2009 Quantum Entanglement and Light Propagation through Bose–Eisntein condensate (BEC) *PhD Thesis* School Bilkent University
[38] Kogelnik H and Li T 1966 *Proc. IEEE* **54** 1312
[39] Inouye S, Pfau T, Gupta S, Chikkatur A, Görlitz A, Pritchard D and Ketterle W 1999 *Nature* **402** 641
[40] Bowden C and Sung C 1978 *Phys. Rev.* A **18** 1558
[41] Bowden C and Sung C 1979 *Phys. Rev.* A **20** 2033
[42] MacGillivray J C and Feld M S 1976 *Phys. Rev.* A **14** 1169
[43] Bonifacio R, Schwendimann P and Haake F 1971 *Phys. Rev.* A **4** 302
[44] Henkel N, Cinti F, Jain P, Pupillo G and Pohl T 2012 *Phys. Rev. Lett.* **108** 265301
[45] Ghazanfari N and Müstecaploğlu Ö E 2014 *Phys. Rev.* A **89** 043619
[46] Das A, Sabbatini J and Zurek W H 2012 *Sci. Rep.* **2** 352
[47] Zhang Y, Bao W and Li H 2007 *Physica* D **234** 49